

Proceedings Article

# Shift coil assembly for a rotating permanent magnet FFL human-scale fMPI imager

A. C. Barksdale<sup>a,b,\*</sup>· E. E. Mason<sup>b</sup>· E. Mattingly<sup>b,c</sup>· M. Śliwiak<sup>b</sup>· J. M. Drago<sup>a,b,d</sup>· L. L. Wald<sup>b,d</sup>

<sup>a</sup>Dept. of Electrical Engineering and Computer Science, Massachusetts Institute of Technology, Cambridge, MA, USA

<sup>b</sup>A.A. Martinos Center for Biomedical Imaging, Dept. of Radiology, Massachusetts General Hospital, Boston, MA, USA

<sup>c</sup>Harvard-MIT Health Sciences & Technology, Cambridge, MA, USA

<sup>d</sup>Harvard Medical School, Boston, MA, USA

\*Corresponding author, email: [alexbark@mit.edu](mailto:alexbark@mit.edu)

© 2022 Barksdale *et al.*; licensee Infinite Science Publishing GmbH

This is an Open Access article distributed under the terms of the Creative Commons Attribution License (<http://creativecommons.org/licenses/by/4.0>), which permits unrestricted use, distribution, and reproduction in any medium, provided the original work is properly cited.

## Abstract

We present the fabrication and characterization of a shift coil assembly designed for a rotating permanent magnet FFL human fMPI imager. The realized system consists of two sets of inner and outer coils (“racetracks”), each driven by an independent amplifier. Hollow conductors and a highly parallel water-cooling circuit provide heat removal during operation. The measured electrical characteristics of the coils ( $R_{inner} = 310 \text{ m}\Omega$ ,  $L_{inner} = 26 \text{ mH}$ ,  $R_{outer} = 399 \text{ m}\Omega$ ,  $L_{outer} = 41 \text{ mH}$ ,  $M = 22.6 \text{ mH}$ ) match simulated values well, and field efficiency measurements demonstrate ability to shift a 1.03 T/m FFL over a 20 cm FOV within driving capabilities of the amplifier system (field efficiency = 0.215 mT/A).

## I. Introduction

Field free line (FFL)-based MPI offers sensitivity advantages from the 2D projection encoding [1]. To create the projection, the FFL must be shifted across the FOV. Although the FFL and its shift could be combined in the same electromagnet system, we separate their generation into a static FFL produced by rare-earth permanent magnets and a shift field generated from electromagnet windings. By doing so, nature stores the energy of the static FFL field, and the electromagnet shift coils can operate using a zero mean AC shift waveform. In this work, we outline the construction methodology and preliminary testing of electromagnet shift coils needed to shift a 1.03 T/m FFL created by a NdFeB permanent magnet assembly across a 20 cm diameter FOV for MPI imaging of a human head (requiring a shift field waveform of

over 100 mT pk). We report measurements of basic coil performance (inductance, resistance, field generation efficiency) for comparison with simulation, compatibility with a four-channel amplifier used for driving this system, as well the water-cooling strategy.

Use of an FFL + shift field to sweep the FFL across the head and produce a projection utilizes relatively low frequency fields, reducing the concern of peripheral or central nervous system stimulation in humans. Thresholds for peripheral nerves increase with frequency (up to at least 100 kHz) and retinal stimulation (the main concern in the CNS) is peaked at about 20 Hz [2, 3]. The rotation of the FFL needed to produce image time-series with a temporal resolution of 3 s oscillates the field at less than 0.4 Hz, and shift fields generating the projection occur on order of 10 Hz, with the upper bound on this frequency to be determined by retinal stimulation thresholds. Based

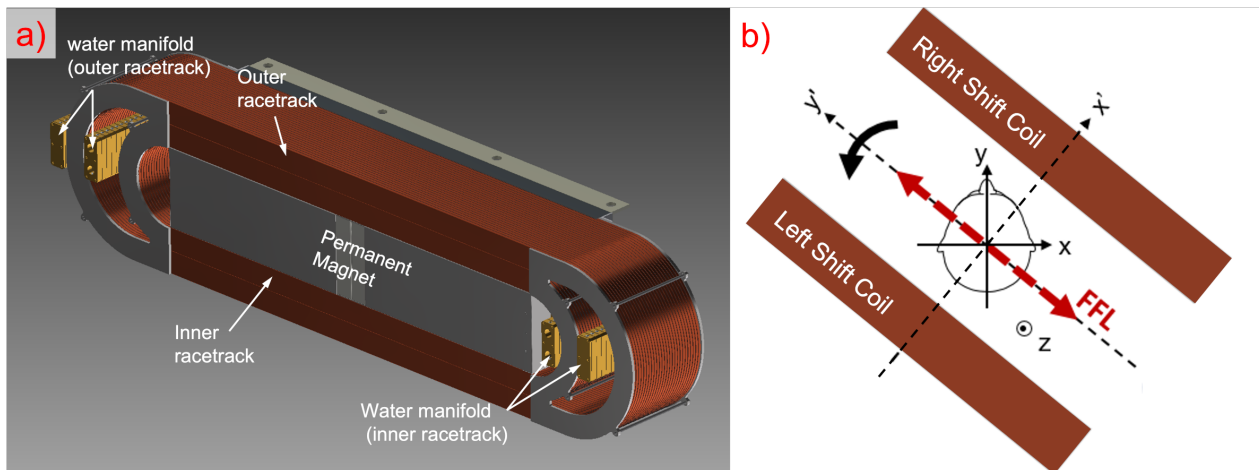


**Figure 1:** a) CAD illustration of permanent magnet FFL and electromagnet shift coil assembly. Each coil consists of an inner and outer set of nested racetracks. Manifolds at the terminals of the coils provide electrical connection and water inlets for cooling. The overall shift coil system will consist of two sets (right and left sides) of the assembly shown in (a) spaced 42 cm. A permanent magnet assembly for creating the FFL is set inside the inner racetrack. b) Reference frames for shift coil rotation. Illustration of a human head (x-y reference frame) and rotating reference frame moving with the shift coils/permanent magnets about z (x'-y' reference frame).

on experiments by Lövsund *et al.*, there is three to four fold increase in the field threshold for magnetostimulation of the retina at 10 Hz when compared to 20 Hz [4]. This leaves only drive frequencies ( $\sim 25$  kHz) as potential sources for nervous system stimulation in humans, which will bound the achievable drive amplitudes [2].

Several considerations and constraints informed the design of the FFL + shift coil assemblies for our human-sized functional brain imaging system [5]. Fig. 1 shows an illustration of one assembly (permanent magnet + racetrack shift coil) and an illustration of both right and left assemblies in the designated coordinate system. The FFL is created by a  $22.5 \times 85 \times 15$  cm<sup>3</sup> permanent magnet with a backplate made of stacked laminated transformer steel. This combination of rare-earth and steel creates an FFL gradient of 1.03 T/m. The shift field is generated from a coil pair (left and right) each formed from hollow conductor (for water cooling) and separated into nested inner and outer racetrack-shaped windings. Separating the windings provides parallelization of the water-cooling circuits. Thus, the total shift assembly has four coils, each independently driven using a custom four channel amplifier, with each channel specified to drive up to 300 A and 750 V, operating up to 100% duty cycle enabling continuous imaging. The amplifier compensation is tuned to handle the self and mutual inductance of the coils. The four-channel amplifier configuration reduces the voltage requirements compared to driving the coils in series and allows the inner and outer racetracks (with different inductances), to have in-phase currents for maximal field efficiency [5].

## II. Material and methods

### II.I. Shift Amplifiers and Data Acquisition

In this work we characterize one shift coil assembly (an inner and outer racetrack pair). It is driven by MPS (Magnet Power Supply) 300-750 amplifiers with a custom power source (IECO Helsinki, Finland). National Instruments PXI-e1073 Chassis with PXIe-6363 and PXIe-6361 DAQ cards (National Instruments, Texas, USA) were used for data acquisition and function generation for shift coil inputs. LabVIEW 2020 (National Instruments, Texas, USA) software was used to interface with the DAQ.

### II.II. Characterization of Shift Coils

Inductance and resistance measurements were performed using an LCR Meter (Agilent 4263B). Inductance was measured at 100 Hz due to the available frequency selection of the meter, and resistance at DC (the shift coil is operated at 10 Hz in this characterization). The IECO MPS 300-750 system provides internal voltage and current monitors which were recorded via LabVIEW. A hall sensor (SS39ET) was used to measure the axial field from the coils. The field efficiency is calculated as the axial field per unit current when driving the inner and outer racetracks with identical amplitude, in-phase current waveforms. Simulated field efficiency for the shift coil in this characterization was performed using Finite Element Method Magnetics open-source software (FEMM 4.2) [6].

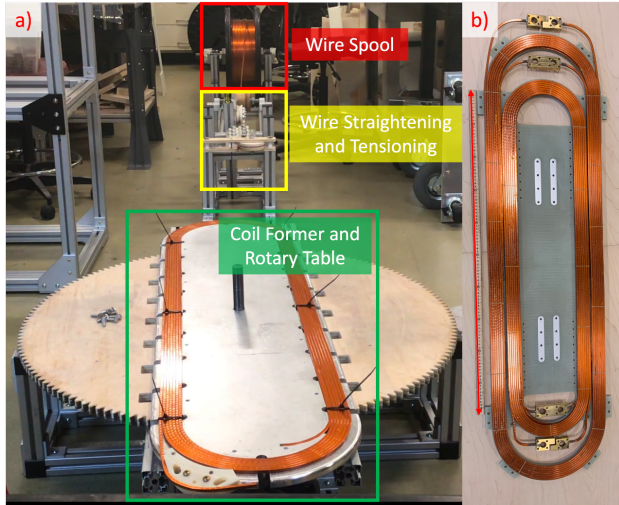


**Figure 2:** a) In house winding jig assembly for shift coils. The winding jig consists of: [red] wire spool containing  $6 \times 6 \text{ mm}^2$  hollow conductor used for shift coil windings, [yellow] wire tensioner and straightener, and [green] coil former and rotary table driven by motor for winding layers b) Finished pancake units (inner and outer racetrack) laid on fiberglass backing support with meter stick lined with red arrow for size reference.

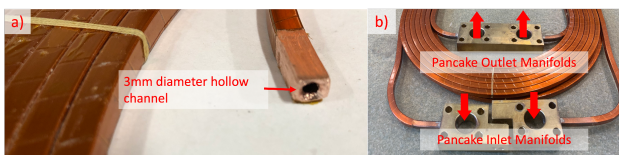


**Figure 3:** a) Close-up of wire used in shift coil winding. A  $6 \times 6 \text{ mm}^2$  conductor with 3 mm diameter hollow channel is chosen to allow water flow for heat removal during operation. b) Single pancake unit showing brass manifolds soldered to the conductor. A pancake unit consists of a set of inlet and outlet manifolds for water flow. When multiple pancakes are stacked, water flows in parallel circuits.

## II.III. Coil Winding and Assembly

The shift coil designs utilize  $6 \times 6 \text{ mm}^2$  square cross-section, insulated magnet wire (1/2 lapped polyimide tape insulation) with a 3 mm diameter hollow channel to enable water cooling (S&W Wire, Cranberry Twp, PA). Each racetrack (of which there are four: inner and outer, for both right and left sides) is composed of 30 stacked layers, with each layer containing 7 turns. The 30 layers is divided into 15 2-layer “pancake” units (spiraling in, then back out). Electrical connection to the coils is achieved with brass manifolds soldered to the unit, which also function as inlets and outlets for water cooling (section II.IV). The stacked pancake units are mechanically clamped together with non-conductive rods and fiberglass backings.

The pancake units were wound in-house using a custom winding jig (Fig. 2). Details of the winding jig can be

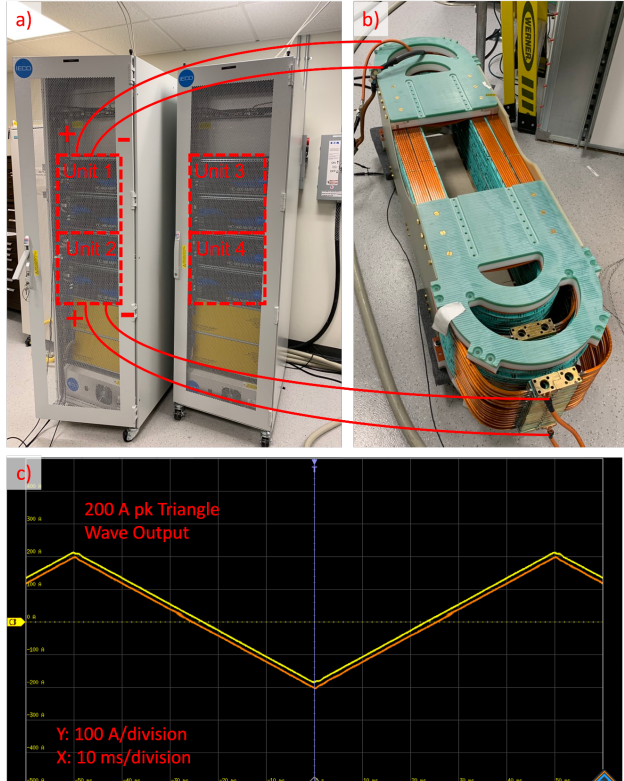


**Figure 4:** a) IECO MPS 300-750 amplifier units. Each tower consists of two amplifier units (each with master and slave amplifier in series). A single 2 channel rack drives a single shift coil (left or right), with each unit driving one racetrack. b) Full shift coil assembly. The red curves drawn from (a) indicate a single amplifier unit powering either the outer racetrack (bottom curves) or inner racetrack (upper curves). c) 200 A pk output current waveform measured from amplifier current monitor. The yellow trace represents current measured from the inner coil in b) and the orange trace represents the outer coil.

found on our open source MPI page [7].

## II.IV. Water Manifolds

Brass manifolds welded to the coils provide inlet and outlets for water flow through the hollow magnet wire. Gaskets custom-cut to the pancake inlets and outlets seal the water within the manifold and provide electrical insulation between layers. Fig. 3 shows detail of the hollow water channel within the wire, and the brass water manifolds. Water flows from the inlet to outlet manifolds such that as pancakes are stacked, inlets and outlets are parallelized to enhance heat removal capacity. For both shift coils dissipating 14.8 kW of heat (250 A pk triangle shift current, apparent power of inner and outer coils utilizing two amplifier units roughly 170 kVA), simulations estimate water cooling at approximately  $3.5 \cdot 10^5 \text{ Pa}$  ( $\sim 0.74 \text{ L/s}$  total volumetric flow rate) will limit heating below 10 °C above inflow temperature (Eq. 13) [8].

**Table 1:** Summary of measured electrical parameters of shift coil assembly and measured field efficiency. Simulated values are also presented for comparison with realized assembly [4]. Note that inductance values were simulated at 7 Hz, while values were measured at 100 Hz due to limitations of the LCR meter.

#### Electric, Magnetic Characterizations

	Inner Racetrack		Outer Racetrack	
Resistance (DC, 25°C)	Measured 310 mΩ	Simulated 301 mΩ	Measured 399 mΩ	Simulated 385 mΩ
Inductance	26 mH (100 Hz)	29 mH (7 Hz)	41 mH (100 Hz)	43 mH (7 Hz)
Mutual Inductance	Measured 22.6 mH (100 Hz)		Simulated 25mH (7 Hz)	
Field Efficiency	0.215 mT/A		0.197 mT/A	

### III. Results and discussion

#### III.I. Shift Coil Characterization

Fig. 4 shows a single shift coil assembly and the four amplifier units housed in two racks. Table 1 presents results from electrical characterizations of the shift coil, measured and simulated values. Fig. 4c shows the measured output (at the coil) of a 200 A pk triangle wave showing good fidelity and performance of the amplifier compensation loop with the input waveform. A hall sensor was placed 21 cm above the top surface of the coils at the center, along the x' axis. This location was chosen to measure field efficiency at the center of the FOV (center of the human head in Fig. 1b), since, in the final design, the two right and left shift coil assemblies will be spaced 42 cm apart (between inner facing surfaces). The field efficiency of the coils for in-phase, identical amplitude current waveforms is shown in Table 1. In the current configuration, a single coil demonstrates a 0.215 mT/A efficiency. When considering the net field for the two coil assemblies, the field efficiency is doubled producing shift fields over 100 mT pk at the amplifier maximum current (300 A pk). This meets the desired shift requirement to translate a 1.03 T/m FFL over a 20 cm FOV.

### IV. Conclusions

The electromagnet shift coils for a human head-sized MPI scanner have been fabricated and characterized.

The measured impedance and field efficiency are presented and compared to simulated values. Current waveforms supplied to the coils by the IECO amplifiers demonstrate the compatibility between the amplifier systems and the shift coil load and ability to shift a 1.03 T/m FFL over a 20 cm FOV. The water circulation system, still under construction, will allow steady state heat removal

and validation of the cooling design.

### Acknowledgments

Funding for the work comes from NIBIB U01EB025121, and NSF GRFP 1122374.

### Author's statement

Conflict of interest: Authors state no conflict of interest.

### References

- [1] Weizenecker, Jürgen & Gleich, Bernhard & Borgert, Joern. (2008). Magnetic particle imaging using a field free line. *Journal of Physics D: Applied Physics*. 41. 105009-. 10.1088/0022-3727/41/10/105009.
- [2] Saritas, Emine & Goodwill, Patrick & Zhang, George & Conolly, Steven. (2013). Magnetostimulation Limits in Magnetic Particle Imaging. *IEEE transactions on medical imaging*. 32. 10.1109/TMI.2013.2260764.
- [3] Lövsund, P. Å. Öberg and S. E. G. Nilsson. (1979). Quantitative determination of thresholds of magnetophosphenes. *Radio Science*, vol. 14, no. 6S, pp. 199-200, Nov.-Dec. 1979, doi: 10.1029/RS014i06Sp00199.
- [4] Lövsund, P., Öberg, P.Å. & Nilsson, S.E.G. (1980). Magneto- and electrophosphenes: A comparative study. *Med. Biol. Eng. Comput.* 18, 758–764. <https://doi.org/10.1007/BF02441902>
- [5] Mason, Erica Ellis. (2020). Magnetic particle imaging for intraoperative breast cancer margin assessment and functional brain imaging. (Doctoral dissertation, Harvard-MIT Program in Health Sciences and Technology).
- [6] D. C. Meeker, Finite Element Method Magnetics, Version 4.2 (21Feb2019 Build), <https://www.femm.info>
- [7] Magnetic Resonance Physics and Instrumentation Group. Open-Source Magnetic Particle Imaging. Retrieved December 12, 2021, from <https://os-mpi.github.io/>.
- [8] Zigrang, D. J., and Sylvester, N. D. (June 1, 1985). "A Review of Explicit Friction Factor Equations." *ASME J. Energy Resour. Technol.* June 1985; 107(2): 280–283. <https://doi.org/10.1115/1.3231190>